HHS Public Access

Author manuscript

J Mol Cell Cardiol. Author manuscript; available in PMC 2021 September 01.

Published in final edited form as:

J Mol Cell Cardiol. 2020 September ; 146: 95–108. doi:10.1016/j.yjmcc.2020.07.004.

Cardiomyocyte cell cycling, maturation, and growth by multinucleation in postnatal swine

Nivedhitha Velayutham[1,2], **Christina M. Alfieri**[1], **Emma J. Agnew**[1], **Kyle W. Riggs**[3], **R. Scott Baker**[3], **Sithara Raju Ponny**[4], **Farhan Zafar**[3,5], **Katherine E. Yutzey**[1,2,6,*]

[1]The Heart Institute, Division of Molecular Cardiovascular Biology, Cincinnati Children's Hospital Medical Center, Cincinnati, OH, USA.

[2]Molecular and Developmental Biology Graduate Program, Division of Developmental Biology, Cincinnati Children's Hospital Medical Center, University of Cincinnati College of Medicine, Cincinnati, OH, USA.

[3]Division of Pediatric Cardiothoracic Surgery, Cincinnati Children's Hospital Medical Center, Cincinnati, OH, USA.

[4]Division of Human Genetics, Cincinnati Children's Hospital Medical Center, Cincinnati, OH, USA.

[5]Department of Surgery, University of Cincinnati College of Medicine, Cincinnati, OH, USA.

[6]Department of Pediatrics, University of Cincinnati College of Medicine, Cincinnati, OH, USA.

Abstract

Background: Rodent cardiomyocytes (CM) undergo mitotic arrest and decline of mononucleated-diploid population post-birth, which are implicated in neonatal loss of heart regenerative potential. However, the dynamics of postnatal CM maturation are largely unknown in swine, despite a similar neonatal cardiac regenerative capacity as rodents. Here, we provide a comprehensive analysis of postnatal cardiac maturation in swine, including CM cell cycling, multinucleation and hypertrophic growth, as well as non-CM cardiac factors such as extracellular matrix (ECM), immune cells, capillaries, and neurons. Our study reveals discordance in postnatal pig heart maturational events compared to rodents.

Methods and Results: Left-ventricular myocardium from White Yorkshire-Landrace pigs at postnatal day (P)0 to 6 months (6mo) was analyzed. Mature cardiac sarcomeric characteristics, such as fetal *TNNI1* repression and CX43 co-localization to cell junctions, were not evident until

*Correspondence to Katherine E. Yutzey, PhD, Division of Molecular Cardiovascular Biology, Cincinnati Children's Medical Center ML7020, 240 Albert Sabin Way, Cincinnati, OH 45229, Katherine.Yutzey@cchmc.org, Phone: 513-636-8340.

Author Contributions

Study design was done by NV, CMA, and KEY. Experimental procedures were executed by NV, CMA, EJA, KWR, RSB, and FZ. Data acquisition, analysis, and interpretation were carried out by NV, CMA, EJA, SRP, and KEY. Figures and manuscript were prepared by NV and KEY. Manuscript was approved for final version by all authors.

Conflict of interest

None declared.

P30 in pigs. In CMs, appreciable binucleation is observed by P7, with extensive multinucleation (4–16 nuclei per CM) beyond P15. Individual CM nuclei remain predominantly diploid at all ages. CM mononucleation at ~50% incidence is observed at P7-P15, and CM mitotic activity is measurable up to 2mo. CM cross-sectional area does not increase until 2mo-6mo in pigs, though longitudinal CM growth proportional to multinucleation occurs after P15. RNAseq analysis of neonatal pig left ventricles showed increased expression of ECM maturation, immune signaling, neuronal remodeling, and reactive oxygen species response genes, highlighting significance of the non-CM milieu in postnatal mammalian heart maturation.

Conclusions: CM maturational events such as decline of mononucleation and cell cycle arrest occur over a 2-month postnatal period in pigs, despite reported loss of heart regenerative potential by P3. Moreover, CMs grow primarily by multinucleation and longitudinal hypertrophy in older pig CMs, distinct from mice and humans. These differences are important to consider for preclinical testing of cardiovascular therapies using swine, and may offer opportunities to study aspects of heart regeneration unavailable in other models.

Keywords

Pig heart development; Large mammal cardiac model; Cardiomyocyte cell cycle; Postnatal cardiac maturation; Neonatal heart regeneration

1. Introduction

Cardiovascular diseases are the leading cause of mortality worldwide, but clinical strategies for effecting regenerative repair in diseased adult human hearts remain elusive [1]. Mouse hearts have been extensively utilized in laboratory research as a mammalian cardiac disease model, but for clinical translation, studies in large mammals such as pigs, dogs, and sheep are mandated. Juvenile pigs, in particular, are often used as a cardiac preclinical model, due to their hemodynamic and anatomic similarity to the human heart [2]. However, fundamental developmental characteristics of the porcine heart, including cardiomyocyte (CM) nucleation, hypertrophic growth, and mitotic arrest after birth, are still minimally characterized.

In the first postnatal week, rodent CMs undergo rapid binucleation and cell cycle arrest, characterized by diminishing expression of mitotic markers, repression of cell cycle-promoting cyclins and cyclin-dependent kinases (CDKs), and cytokinesis failure [3, 4]. At the same time, CMs switch from hyperplastic to hypertrophic mode of growth, identified by increased cross-sectional area [5]. There is also concurrent decline of mononucleated-diploid CMs with a corresponding increase in binucleation [5, 6]. Further, sarcomeric maturation and induction of oxidative metabolic pathways also occur in the first two postnatal weeks in rodent hearts. Alongside these CM maturational processes, there is also increased extracellular matrix (ECM) deposition and stiffness, vascular capillary growth, sympathetic neuronal maturation, and immune cell signaling [7–12]. Thus, by 2–3 weeks after birth, rodent hearts are terminally mature, growing primarily by CM hypertrophy and forming fibrotic scar upon injury [13]. Each of these maturational events have also been identified in rodents as targets for regulation of neonatal regenerative potential after birth.

Recent reports show that swine, similar to rodents, have a transient heart regenerative capacity in the first few days after birth [14, 15]. However, the timing and sequence of cardiac maturational events after birth are unknown in swine. Also, though pigs are widely used in preclinical studies for cardiac therapeutics [2], there is a dearth of knowledge in pig CM growth dynamics, particularly in the postnatal period. Direct comparison of postnatal growth mechanisms between swine and rodents could thus help establish the conserved processes underlying CM terminal maturation and loss of cardiac regenerative potential in large and small mammals after birth, facilitating clinical translation to humans.

In this study, we provide a comprehensive characterization of heart development up to 6 months after birth in swine. Our results describe the sequence of events involved in postnatal cardiac terminal maturation, in this important large mammalian model. We investigated CM characteristics including cell cycle arrest, nucleation, and hypertrophy in postnatal pigs. Our data show discordance in the timing of CM terminal maturation, compared to reported loss of heart regenerative potential [14, 15], in swine. Also, the CM growth dynamics involved in increased nucleation and transition to hypertrophic growth are distinctive in pigs, from rodents and humans. Moreover, RNA sequencing (RNAseq) for myocardial gene expression profiling in postnatal pigs showed upregulation of genes involved in ECM, immune, and neuronal maturation as well as reactive oxygen species (ROS) response. These data in swine add support to the importance of physiological and local microenvironment cues, in regulating cardiac terminal maturation and regenerative capacity after birth in mammals.

2. Methods

An abbreviated methods section with key experimental details is provided below. The expanded methods section can be found in the online supplementary data file. Details on antibodies and reagents, including dilutions, working concentrations, and manufacturer information, are provided in Supplementary Table 1. Primer sequences used for RT-qPCR are listed in Supplementary Table 2. RNAseq differential expression analyses are available in Supplementary Table 3.

2.1 Pigs

All experiments with animals were performed conforming to NIH Guidelines on Care and Use of Laboratory Animals. All protocols involving animals were approved by the Cincinnati Children’s Hospital Institutional Animal Care and Use Committee (IACUC). A total of n=68 White Yorkshire-Landrace farm pigs were utilized in this study, with n=14 pigs per stage at P0 to P30, n=4 at 2mo, and n=8 at 6mo. Male and female pigs were included in all analyses.

2.2 Tissue harvest and processing

After euthanasia, cardiac left ventricular free wall tissue was obtained for analysis. Freshly harvested tissue was washed in 1X phosphate buffered saline (PBS) and placed in 4% paraformaldehyde (PFA) for histology, in 3.7% formaldehyde for CM dissociations, or flash-frozen in liquid nitrogen for mRNA and protein studies.

2.3 Cardiomyocyte dissociations

The protocol of Mollova *et al.* [16] was modified for isolating individual CMs from pig left ventricular tissue. Following 3.7% formaldehyde fixation, heart pieces were digested in freshly-prepared Collagenase mixture. Eluate was filtered and gently centrifuged (800rpm, 2 minutes) to obtain CM pellets, which were resuspended in 1X PBS. Antibody staining was performed in cell suspensions by repeated pelleting of CMs after each step. Following staining, CM pellets were resuspended in Vectashield Hardset mounting medium and placed onto slides using coverslips, then dried overnight before imaging. A modified method from Patterson *et al.* [17] was used for ploidy assessment of Hoechst-stained CM nuclei.

2.4 Immunofluorescence staining

Wheat Germ Agglutinin (WGA, Alexa Fluor 647 conjugate or TRITC conjugate) was utilized to stain for cardiac cell membranes. Nuclei were visualized by DAPI or Hoechst 33342. Gap junctional maturation was visually assessed by co-localization of Connexin-43 (Cx43) to intercalated discs. Mitotic indices were calculated by counting nuclear Phosphohistone-H3 Ser10 (pHH3) expression in CMs identified by α-actinin (CM sarcomere) or PCM1 (CM nuclei). Desmin was also used to visualize CMs. Vimentin staining identified non-CM populations in ploidy quantification experiments. Staining quantification, object counting, and morphometric analyses were performed using NIS Elements and Fiji (ImageJ) software. Information on antibody catalog numbers and dilutions are provided in Supplementary Table 1.

2.5 mRNA analysis by RT-qPCR

Ventricular mRNA was extracted using NucleoSpin RNA kit. Following cDNA synthesis, RT-qPCR was performed using SYBR Green. Gene-specific primer sets, designed with NCBI PrimerBlast, were validated by Sanger sequencing (Supplementary Table 2). Relative gene expression was calculated by comparative $\Delta\Delta Ct$ method [18], with *18S* ribosomal RNA used for normalization. Normalized average expression of P0 was set to 1.0 to calculate fold change after birth.

2.6 RNAseq analysis

Total RNA isolated from pig left ventricular myocardial tissue at P0, P7, and P15 (n=3 per stage) was used. Trimmed reads from FASTQ files were mapped to the Sscrofa11 (swine) reference genome using Hisat2 for reference alignment [19]. Transcriptome index created in Kallisto was used to quantify transcripts per million (TPM), and RUVSeq was used to perform differential gene expression analyses between groups [20]. Significant differentially expressed genes were obtained using a fold change cutoff of 2 and adjusted p-value cutoff of ≤0.05. Downstream functional annotation and pathway analysis were determined using ToppFun tool from the ToppGene Suite [21], and heatmaps were generated using the Morpheus web-tool. An adjusted p-value cutoff of ≤0.05 was used to select functional annotations and pathways. Data files are available in the GEO database (GSE145346).

2.7 Statistics

Statistical analyses were performed using GraphPad Prism 8 software, by unpaired One-way ANOVA non-parametric Multiple Comparisons tests, such as Kruskal-Wallis tests with Dunn's corrections or Brown-Forsythe and Welch tests with Games-Howell corrections. $p<0.05$ was deemed significant.

3. Results

3.1 Cardiac sarcomeric and gap junctional maturation occur beyond P30 in pig hearts

To assess cardiac maturational transitions in the weeks after birth, pig hearts were collected at P0 (postnatal day 0), P7, P15, P30, 2mo (2 months post-birth) and 6mo (6 months post-birth), to span birth, weaning, and adolescent ages (Figure 1A), similar to the 1-month period of cardiac terminal maturation in mice [22] (Figure S1A–B). Both cardiac and total body weights significantly increased beyond P30 in pigs (Figure S2A–C), and heart weight-to-body weight ratios were only decreased by 6mo (Figure 1B). These data indicate disproportionate body weight increase relative to heart growth at 2–6mo in pigs. Assessing left ventricular morphology and maturation, WGA staining in pig hearts revealed presence of 'fetal-like' CMs with large central nuclei up to P30 (Figure S2D). Nuclear density, determined by number of DAPI-stained nuclei per cross-sectional CM area as an approximation of cell density, was also not significantly reduced until 6mo (Figure S2E). Fetal contractile protein isoforms *TNNI1* and *MYH6* are still detectable at P30 and 2mo respectively in pigs, while significant upregulation of mature contractile protein isoforms *TNNI3* and *MYH7* did not occur until 6mo (Figure 1C–D). Note that in pigs, like humans, MYH7 is the predominant mature myosin heavy chain isoform, whereas MYH6 predominates in adult mice [7]. Also, CM gap junctional maturation by localization of Cx43 to intercalated discs is not evident until P30 in pigs (Figure 1E, Figure S2F). Complete junctional maturation is observed only by 2mo to 6mo, although immature lateral punctate Cx43 expression is still seen at 2mo. In contrast, mouse cardiac gap junctional and sarcomeric maturation, indicated by co-localization of Cx43 to intercalated discs (Figure S1C) [23, 24] and downregulation of fetal contractile protein isoforms (*Tnni3* and *Myh6*) (Figure S1D–E), occur concurrently with loss of regenerative potential [7, 24], by P7-P15. Together, these data suggest that, despite a similar neonatal heart regenerative period in pigs and mice, cardiac sarcomeric maturation occurs over 2–6 postnatal months in pigs, as opposed to 2–3 weeks in mice.

3.2 Pig cardiomyocytes are progressively multinucleated from P15 to 6mo, with significant mononucleation at P15

In mice, CM binucleation begins in the first week after birth and nearly all CMs are binucleated by P15, which is maintained in the adult murine heart [6]. While existence of multinucleated CMs has been reported in young-adult pigs [25], CM transitional dynamics towards a multinucleated state are not well-defined in swine, particularly in the first few months after birth. We assessed nucleation in dissociated CMs isolated from pig left ventricles at P0 to 6mo. Individual CMs dissociated from formalin-fixed left ventricular tissue were stained with α-actinin and DAPI, for quantification of number of nuclei per CM (Figure 2A–B). At birth, pig CMs are mostly mononucleated (~90%), with a small

population having two nuclei per CM. This indicates prenatal onset of binucleation in a small fraction of CMs in pig hearts. Interestingly, a significant population of mononucleated CMs (~75–50%) are retained until P15, but only ~10% of CMs are mononucleated by P30. Unlike rodents, pig CMs become multinucleated, with ~5% tetranucleation (4 nuclei per CM) at P15, progressing to prevalence of 8–16 nuclei per CM by 6mo. In tissue sections of pig hearts at 2mo and 6mo, multinucleated CMs could be identified by WGA staining for CM boundaries (Figure 2C). Thus, pig hearts exhibit onset of CM multinucleation by P15-P30, with maintenance of significant CM mononucleated population in the first two weeks after birth.

3.3 Cardiomyocytes are mitotically active up to 2mo in pig left ventricles

CM cell cycle arrest in the first week after birth [3, 4, 6] is a significant hallmark of loss of regenerative capacity in rodent CMs. To determine timing of cardiac cell cycle arrest in postnatal pigs, mitotic indices were assessed by pHH3 (mitotic M-phase marker) staining. Nuclear pHH3 counts revealed nearly 0.1% of CM nuclei are mitotically-active up to 2mo in pigs (Figure 3), with no significant decrease in pHH3 levels until 6mo compared to neonatal stages (Figure 3B). Thus, pig CMs remain capable of active cell cycling up to 2 postnatal months. By two independent analyses, utilizing sarcomeric α-actinin (Figure 3) and perinuclear PCM1 staining (Figure S3A–B) to accurately identify CMs, the highest pHH3 expression (~0.3%) in CMs was measured at P7-P15 in pigs. This postnatal increase in CM mitotic activity is concurrent with increased numbers of bi- and multi-nucleated CMs, suggesting multiple rounds of nuclear division (karyokinesis) without cell division (cytokinesis) at these stages. Interestingly, karyokinesis in the absence of cytokinesis could also be visualized in longitudinal sections of older pig hearts, with simultaneous activation of pHH3 seen in adjacent nuclei of multinucleated CMs (Figure 3C). Thus, mitotically-active CMs are present up to 2mo in pig hearts, with karyokinesis in the absence of cytokinesis occurring in multinucleated CMs.

3.4 Individual nuclei in pig cardiomyocytes remain predominantly diploid by 6 months after birth

Postnatal CM polyploidization has been implicated as a mechanism for loss of proliferative capacity in the adult mammalian heart in rodents [17, 26]. CM polyploidization occurs chiefly by binucleation in mice, with individual CM nuclei being mostly diploid (2c) [17]. Meanwhile, humans exhibit mononucleated CMs with polyploid (>2c) nuclear DNA content [27]. In pigs, overall CM polyploidization occurs via bi- and multi-nucleation from P0–6mo (Figure 2). But ploidy of individual nuclei in postnatal pig CMs is unknown. We measured DNA content of individual nuclei in pig CMs by Hoechst staining, using two independent methods.

In dissociated cell preparations, CM nuclear Hoechst intensity was normalized to sperm nuclear intensities serving as technical control per area (Figure S4A). We found that the ratios of normalized Hoechst intensities between CM and sperm nuclei did not significantly change across various pig ages and extent of CM nucleation (Figure S4B). This indicates that the DNA content per nucleus observed at P0 in mononucleated CMs is predominantly the same as the DNA content per nucleus observed in a 2mo mononucleated CM or in a 6mo

multinucleated CM. Thus, our results in dissociated CMs indicate that DNA intensity per nucleus does not change after birth in pigs.

To quantify actual 2c and >2c DNA content in pig CM nuclei, Hoechst intensity was measured in left ventricular cryosections co-stained with Desmin (CM) and Vimentin (non-CM). Vimentin-positive cell nuclei was utilized as internal 2c control for relative intensity measurements per field (Figure 4). Thresholds for 2c and >2c cut-offs were determined as described in supplementary methods, based on published studies [17, 26]. We found no significant change in relative Hoechst intensities from P0 to 6mo (Figure 4A–B), indicating individual pig CM nuclei are mostly diploid in the first six postnatal months. When percentages were estimated, approximately 90% of CM nuclei were within the normalized threshold for diploid DNA content (Figure 4E). These percentages are comparable to a previously reported study, which found 75%−85% diploid CM nuclei in adult pig hearts [28]. Further, measuring nuclear Hoechst intensities in multinucleated CMs of longitudinal cardiac cryosections also revealed primarily diploid nuclear DNA content (Figure 4C–D). This supports our observation in dissociated pig CMs (Figure S4) that there is no change in DNA content per nucleus in multinucleated CMs after birth. Together, these data show the predominance of diploid (2c) DNA content per nucleus in mono-, bi- and multi-nucleated CMs from P0–6mo in pigs.

3.5 Longitudinal growth with multinucleation precedes hypertrophic growth by width in postnatal pig cardiomyocytes

A characteristic event in transition of the neonatal heart to a terminally-differentiated adult heart in rodents is the switch from hyperplastic to hypertrophic CM growth [5]. To evaluate when CM hypertrophic growth is initiated in pig hearts at P0-P60, we measured CM area in left ventricular paraffin sections and in dissociated heart CM preparations. Cross-sectional area (CSA) was assessed in pig left ventricular tissue stained with WGA and DAPI. There was no significant change in CM circumference between P0 and P30 in pigs (Figure 5A–B). By 2mo, CSA showed an increasing trend, with significant CM expansion by CSA only seen by 6mo (Figure 5B). When total cell surface area (TSA) was measured in 2D images of dissociated CMs stained with α-actinin, there was no significant increase from P0 to P15 (Figure 5C–D). By P30 and beyond, TSA was significantly increased in multinucleated CMs. Additionally, measurements of length and width in dissociated CMs showed longitudinal (lengthwise) growth in multinucleated CMs at all stages, with increased length relative to number of nuclei per CM (Figure 5E–F). However, increased CM width was only significant by 2mo-6mo. Further, to demonstrate that increased CSA at 2mo-6mo in paraffin sections is not due to technical variations in plane of sectioning, we compared CM CSA (cytoplasmic area) against cross-sectional nuclear area measured in the same region (Figure 5G). The average cross-sectional area per nucleus does not change across stages, while CM CSA alone increases with age, validating our observations. Together, these data demonstrate a distinct mode of CM growth in pigs, with longitudinal CM growth relative to multinucleation after P15, and diametric CM growth by significantly increased cross-sectional area occurring at 2mo-6mo.

3.6 Transcriptional changes in postnatal pig hearts by RNAseq

Our results show that pigs exhibit a prolonged 2mo-6mo period of CM mitotic arrest and terminal maturation (Figures 1–5), which is discordant from recently reported loss of heart regenerative capacity in pigs at P3 [14, 15]. This is unlike mice, where CM cell cycle arrest and maturation occur in the first postnatal week, coincident with loss of regenerative potential [13]. In mice, apart from CM activity, maturational processes of non-CM cardiac cell populations (immune cells, fibroblasts, vascular capillaries), as well as ECM and metabolic changes, are implicated in postnatal heart maturation and loss of regenerative potential. The timing and pattern of these maturational processes are not known in postnatal pigs. Hence, we assessed global transcriptional changes in neonatal pig hearts by RNAseq. Total RNA isolated from pig left ventricular tissues at P0, P7, and P15 was analyzed to span the reported timepoints of regenerative and non-regenerative ages in pigs (Figure 6A).

Hierarchical dendrogram and principal component analysis both showed clustering of biological replicates primarily within their own stages, with some overlap at P7-P15 indicating similarities in transcriptional profiles between these stages compared to P0 (Figure S5A–B). Overall, about 2250 genes were significantly dysregulated (significant up- or down-regulation in any of the comparison groups) between birth and 2 postnatal weeks in swine (Figure 6B). The 100 most dysregulated genes were primarily involved in ion transport and signal transduction (Figure S5C). Three comparison groups for differential expression analyses were chosen as P7 vs. P0 (up- or downregulation of genes at P7 compared to P0), P15 vs. P0, and P15 vs. P7. Gene Ontology (GO) enrichment was performed for all comparison groups using ToppFun tool [21] to obtain significant Biological Process GO terms (GO-BP). Genes involved in cell cycling, immune signaling, ECM organization, neuronal remodeling, and metabolic processes were significantly dysregulated in pigs after birth (Figure 6B).

3.7 Upregulation of mitotic activity at P7 and downregulation of cytokinetic genes by P15 in pig ventricles

Analyzing individual comparison groups, in P7 vs. P0, top GO-BP terms were associated with mitotic processes, indicating cell cycle genes are significantly upregulated by P7 in pig left ventricles (Figure 6C). This supports our observation of increased mitotic activity in pig CMs after birth (Figure 3, Figure S3). In particular, Cyclins and CDKs promoting S/G2/M transitions, such as *CCNE2*, *CCNA1*, and *CCNB2* are upregulated after birth, while G1-phase genes such as *CCND1* and *CDK4* showed similar levels of expression at P7 and P15 (Figure S6A–B). These findings were validated by RT-qPCR, showing repression of cell cycle genes only by 2mo-6mo after birth in pigs (Figure S6C). This is in contrast to mice, where S/G2/M-specific *Cyclins* and *CDKs* are significantly downregulated by P7-P15 (Figure S7). However, some cell cycle processes are downregulated in pigs between P7 and P15, particularly cytokinetic genes such as *AUNIP*, *ANLN*, *AURKB* (Figure S6A). Interestingly, *ECT2* and *LMNB2*, loss of which is implicated in cytokinesis failure and promotion of CM polyploidization in rodents, are also downregulated soon after birth in pigs [29, 30]. Additionally, cardiac developmental and proliferative pathway genes [31] were examined by protein quantification and RNAseq. AKT phosphorylation and β-catenin protein levels, both implicated in cardiomyocyte proliferation in mice, were maintained in

the weeks after birth in swine relative to P0 levels, and were also not significantly decreased until 6mo (Figure S8). However, downregulation of some genes associated with CM proliferative capacity, such as *BMP10* and *FOXM1,* occurred by P7 and P15 respectively (Figure S8E) [31, 32]. Thus, CM mitotic activity and expression of developmental and proliferative pathway genes are maintained after birth until 2–6mos in pig hearts. Interestingly, genes downregulated in cytokinesis failure are also significantly downregulated by P7-P15, consistent with the timing of CM multinucleation onset in postnatal swine.

3.8 Upregulation in immune signaling and downregulation of monocarboxylic acid metabolic process in postnatal pig hearts

By Venn diagram intersections between the three comparison groups, 779 overlapping significantly upregulated and 322 overlapping significantly downregulated genes were identified (Figure S9A,C). GO-BP terms for all common overlapping genes showed upregulation in immune signaling and downregulation in monocarboxylic acid metabolic processes after birth in pigs (Figure S9B,D).

In P15 vs. P0 and in P15 vs. P7, top GO-BP terms for significantly upregulated genes were involved in immune signaling (Figure 6E–F, Figure S9E–F). Upregulated genes, including *MAP3K5*, *CX3CR1*, and *CXCL12*, are primarily involved in innate immune response and maturation, via inflammatory chemokine/cytokine signaling (Figure S10A). Staining for CD45 (hematopoietic lineage marker) in pig left ventricles showed a significant increase in CD45+ cell populations by P15, supporting RNAseq results (Figure S10B–C). Thus, cardiac innate immune signaling is upregulated in the first two weeks after birth in swine.

In all comparison groups, top GO-BP terms for significantly downregulated genes were associated with carboxylic acid metabolic processes. Carboxylic acid processes, including Krebs (tricarboxylic acid) cycle, modulate the intermediate steps between glucose and beta-oxidation metabolic transition [33]. Downregulation of carboxylic acid processes after P0 suggests transition to oxidative metabolism likely occurs in late gestation in pigs, with active transcription of intermediate metabolic processes declining in the first few neonatal days. Supporting this, we see comparable transcriptional activity and gene expression maintenance of both glycolysis and beta-oxidation genes in the first postnatal month in swine, both by RNAseq and by RT-qPCR (Figure S11). In mice, there is switch from glycolysis to beta-oxidation by P7 compared to P0 [34]. Alongside this, repression of fetal-like glucose transporter gene *Slc2a1* and upregulation of mature *Slc2a4*, indicative of CM terminal maturation [35], occur by P7-P15 in mice (Figure S12). In pigs, however, reduced *SLC2A1* and increased *SLC2A4* expression are only significant by 2mo-6mo (Figure S11C,F). Our data indicate that glycolytic and beta-oxidation metabolism genes are expressed together in the first postnatal month. This suggests that, unlike mouse hearts, there is no clear switch from fetal-like glycolytic to mature beta-oxidation metabolism in the neonatal period in pig hearts.

3.9 Increased ECM maturation, ROS response, and neuronal remodeling in pig hearts after birth

By GO-BP analysis, we see significant modulation of immune and metabolic signaling in postnatal pigs (Figure 6). Apart from these processes, other cardiac microenvironment factors like ECM composition and mechanical stiffness, angiogenic factors, ROS increase, and neuronal signaling, are also implicated in cardiac maturation and regenerative potential after birth in rodents [13]. We thus investigated significant transcriptomic changes in these processes after birth in our pig RNAseq dataset.

In mice, collagen maturation, as indicated by upregulation of collagen mRNA isoforms as well as by Collagen Hybridizing Peptide (CHP) staining for collagen protein remodeling, is increased by P7 (Figure S13A–C). In pigs, by P7, RNAseq analysis showed significant upregulation of ECM maturation genes (Figure 7A). Important fibrillar collagen isoforms such as *COL1A1* and *COL3A1* were not significantly differentially expressed at P0-P15 in swine, but their expression was maintained until 2mo (Figure S14A–B). Interestingly, ECM isoforms that are considered fetal-like, such as *COL3A1* and *FN1*, were upregulated after birth in pigs, with no significant downregulation in expression until P30–2mo (Figure S13A–B). However, collagen deposition and maturational remodeling, which results in stiffening of the matrix, was evident by P7-P15 in pig hearts by CHP staining (Figure S13C–E). Thus, while pig hearts retain mRNA expression of fetal-like ECM components until 2mo, fibrillar collagen deposition and ECM remodeling is initiated by P7.

There is an increasing trend for vascular density in the first two postnatal weeks in mice, as seen by Lectin-DAB counts for capillaries (Figure S13D–E). Pigs, however, show downregulation after birth of genes involved in neovascularization and sprouting angiogenesis, such as *VEGFA* and *VASH1* (Figure 7B). By Lectin-DAB capillary counts in swine, we also observed no significant postnatal increase in vascular density (Figure S15). Therefore, pig myocardial vascular density is established before birth. ROS responsive genes, particularly those involved in DNA damage repair and oxidative stress response, are upregulated by P7 in pig hearts (Figure 7C), similar to mice. However, *HIF1A* levels does not significantly change in the postnatal period but shows maintained transcriptional activity (Figure S16), suggesting late gestation induction of *HIF1A* signaling in pigs. Cardiac innervation is shown to mediate CM proliferative capacity in rodent [36]. Characterization of neuronal remodeling after birth in swine showed significant upregulation of genes regulating neuronal connectivity and synaptic signaling such as *TENM1*, *TENM3* and *NAV3*, by P7-P15, while neurite growth and adhesion genes were downregulated after birth (Figure 7D). Expression of Tyrosine hydroxylase (TH), which is highly expressed in the sympathetic nervous system and involved in synaptic signaling of adrenergic nerve fibers was examined as an indicator of sympathetic innervation post-birth. We observed increased trend for TH expression after birth till P15, with subsequent downregulation at P30 (Figure S17), These data indicate increased neuronal remodeling in the first two postnatal weeks in pig hearts.

Our data collectively show that, while vascular density in the rapidly-growing postnatal pig heart does not change, there is increase in cardiac ECM remodeling, ROS response, and

neuronal activity by P7-P15, coinciding with loss of postnatal heart regenerative potential, in swine.

4. Discussion

Here we report a comprehensive analysis of cardiac myocyte and non-myocyte maturational dynamics in postnatal swine. Our results show that CM maturation, including mitotic arrest, decline of mononucleated-diploid CMs, and sarcomeric isoform switching, occurs over a 2 to 6-month postnatal period in pigs, despite reported loss of regenerative potential by P3 [14, 15]. This contrasts with mice where CM mitotic arrest and maturation occurs at the same time as loss of regenerative potential (Figure 8). Thus, our results show a discordance in the relative timing of CM postnatal maturation and loss of heart regenerative potential in swine compared to rodents. In contrast, RNAseq analysis revealed upregulation of innate immune signaling, ROS response, ECM maturation, and sympathetic neuronal signaling in the first two weeks after birth in pig left ventricles, similar to rodents. Thus, such microenvironment cues, implicated in postnatal cardiac maturation of both mice and pigs, could underlie the similar regenerative periods in these species. A unique feature of pig CMs is extensive CM multinucleation after P15, by nuclear division in the absence of cytokinesis. Also, CM growth by longitudinal elongation occurs after P15, with CM circumferential hypertrophy only observed by 2mo-6mo. Such distinctive CM growth characteristics should be considered in preclinical and translational studies using swine as a large animal model for human cardiovascular disease.

4.1 CM mitotic activity and progressive multinucleation in postnatal pigs

CM cell cycle arrest occurs in the first postnatal week in rodents, concurrent with loss of regenerative capacity, resulting in negligible CM proliferation and myocardial loss after injury in adults [27, 37]. Inducing cell cycle re-entry in CMs has thus been tested as a mechanism for effecting cardiac regeneration, based on murine models [38]. We show here that karyokinesis in the absence of cytokinesis occurs in the multinucleated CMs of postnatal pigs. Thus, translation of findings from mice to large mammals will need to extend beyond induction of CM cell cycle re-entry alone as a measure of cardiac proliferative repair after injury, particularly in preclinical models that have significant CM multinucleation. In addition, studies of large mammals that exhibit CM multinucleation may not be comparable to humans with predominantly mononuclear-polyploid CMs. Assays for CM nucleation/ploidy as well as *in vivo* measurement of cytokinesis will be required in large mammal preclinical studies, to confirm cardiac healing via CM proliferation. Further, *LMNB2* and *ECT2*, both reported to mediate cytokinesis failure and increased CM nucleation and ploidy in rodents [29, 30], are downregulated by P7-P15 in pig hearts. These could be key conserved mechanisms in mammals that mediate postnatal CM cytokinesis failure and transition to bi/multinucleation. A recent study revealed the possibility of forcibly-inducing cytokinesis in multinucleated CMs by manipulating β-catenin levels in hypoxic mice [39]. Since adult and diseased human hearts mostly display patterns of increased CM nucleation and ploidy, induction of cytokinesis in polyploid CMs would be an exciting therapeutic strategy. Exploring the mechanisms driving CM proliferation and multinucleation in the pig

model could thus provide unique insights into postnatal CM proliferative capacity and cytokinetic arrest in large mammals.

4.2 Discordance in timing of CM maturational events compared to loss of regenerative potential in swine

Recent studies indicate that neonatal pigs possess a P0-P3 window of cardiac regenerative potential, and that injury at P7 or P14 leads to extensive scarring [14, 15]. In mammals, the inability of the heart to regenerate is strongly correlated to the lack mononucleated-diploid CMs [40]. The innate capacity of zebrafish and newts for heart regeneration throughout life is linked to presence of mononucleated-diploid CMs [41], and CM polyploidization is sufficient to inhibit cardiac regeneration in zebrafish [17, 42]. Here, we show that pig hearts exhibit over 50% CM mononucleation at P15, even though heart regenerative capacity is lost beyond P3. Recently published results from our lab also show a lack of regenerative capacity in P30 pig hearts subjected to transient ischemia/reperfusion injury [43], despite cell cycle activity and ~10% incidence of CM mononucleation at this age. Also, characteristics of terminally-mature cardiac sarcomeres, such as repression of *TNNI1* and *SLC2A1*, gap junctional maturation, and complete transition to hypertrophic mode of growth, occur after P15 in pig hearts. Thus, CM maturation is disconnected from regenerative potential in postnatal pigs.

ROS-mediated oxidative stress signaling and switch to beta-oxidation are important CM maturational events in postnatal mice [8], and a hypoxic, low-ROS cardiac environment is more conducive for regeneration via CM proliferation [44]. Our data show that many ROS-responsive DNA repair pathways are upregulated in the first postnatal week in pig hearts, coincident with loss of regenerative potential. However, expression of *HIF1A* and *MEIS1*, important regulators of oxidative stress response and cell cycle arrest, are not significantly upregulated after birth in pig left ventricles. Similarly, we see no clear transition to beta-oxidative metabolism occurring postnatally in pig hearts. In sheep, the switch to beta-oxidation initiates by mid-to-late gestation *in utero*, alongside onset of CM binucleation [45, 46]. Considering the incidence of ~10% binucleation at birth in pigs, as well as placental permeability to free fatty acids [47], the transition to oxidative metabolism is likely also initiated before birth in pig hearts. Currently, cardiac growth dynamics during mid- to late-gestation in pigs is not known. Studying cardiac maturation and regenerative potential pre- and postnatally in pigs and other large mammals will be informative to identify critical parameters for cardiac maturation and regeneration in the mammals.

4.3 Cardiac non-CM cell populations and tissue organizational networks undergo maturational remodeling at P7-P15 in swine

In addition to CM maturational events, contributions of non-CM cardiac factors are important in regulating heart regenerative potential in rodents. These include maturation of cardiac fibroblasts, ECM composition and rigidity, macrophages and other immune cell signaling, vascular capillary growth, and sympathetic neuronal innervation, [9, 10, 12, 36, 48]. In mice, postnatal increase in ECM stiffness is linked to CM proliferative withdrawal, and presence of fetal-like ECM factors are necessary for cardiac regenerative repair [9]. Increased vascularity is also a concurrent process in postnatal rodents, and angiogenic

mechanisms are implicated in mouse heart regenerative potential [10]. In postnatal pigs, similar to mice, we observe significant upregulation of genes involved in ECM maturation by P7, alongside robust collagen remodeling. However, in contrast to mice, ECM genes that are considered 'fetal-like' such as *COL3A1*, and known to promote heart regenerative repair such as *FN1* and *AGRN* [48, 49], are still transcriptionally active at P7-P15 in swine. Both *FN1* and *COL3A1* gene expression are not significantly reduced until 6mo in pigs. It is possible that maintained expression of these 'immature' ECM isoforms is necessary for all CM cell cycle activity, whether it is proliferation or endoreplication. Also, unlike mice, vascular density does not change in postnatal pig hearts, indicating myocardial vascularization is established before birth in swine. Innate immune maturation and sympathetic neuronal signaling are upregulated in the first two postnatal weeks in swine, following loss of heart regenerative capacity and coincident with transition to a multinucleated CM state. There is evidence of crosstalk between inflammatory and neuronal signaling in regenerative healing in rodent hearts [36]. Studying the direct regulatory roles and targets of these conserved processes in mouse and pig hearts are important future avenues to understand postnatal mammalian cardiac maturation and regenerative repair.

4.4 Is there an optimal animal model for preclinical studies of human heart disease?

Juvenile pigs at 2mo-6mo are popular models in preclinical cardiac studies, as FDA regulations mandate use of large mammals to test cardiac therapies [46]. As we show here, pig hearts are still actively undergoing maturational remodeling during this postnatal period. Further, our study highlights fundamental variations in pig CM characteristics such as multinucleation and differential mechanisms of hypertrophy and cell cycling, compared to rodents and humans. Across vertebrate species, CMs are predominantly mono- or bi-nucleated, with some CM tetranucleation reported in sheep and dogs [26, 46]. In pigs, however, we see 8–16 nuclei per CM by 6mo, with up to 32 nuclei per CM reported in older swine [25]. Also, CM growth in swine occurs by increase in length relative to nucleation during juvenile and adolescent stages, prior to the increase in width. This mechanism of longitudinal CM growth is previously unreported in mammals, but has been recorded in chickens supporting differential myocardial growth mechanisms in diverse species [50]. Thus, there exist fundamental differences in CM biology and growth dynamics in pigs, that are not seen in other mammals such as mice and humans. These may prove important to consider while designing preclinical tests for cardiac regenerative therapeutics using swine. Further, as strain-specific variations have proven important considerations in mouse CM biology and regenerative potential [17], there are likely differences between our model of White Yorkshire-Landrace pigs compared to other commonly-used swine breeds for biomedical research, specifically miniature pig breeds such as Yucatan, Hanford, Sinclair, and Göttingen [2]. Ultimately, there may not be a single mammalian model that recapitulates the human heart. However, investigating such differences in pigs and other mammals could offer unique opportunities to study diverse aspects of CM proliferation and cardiac regeneration, thereby enhancing clinical translatability of therapies for human heart disease.

Supplementary Material

Refer to Web version on PubMed Central for supplementary material.

Acknowledgements

We thank Dr. Bernhard Kühn (UPMC Children's Hospital, Pittsburgh) for providing cardiomyocyte dissociation protocols, and Dr. Michaela Patterson (Medical College of Wisconsin, Milwaukee) for critical suggestions in optimizing ploidy assessment in pig cardiomyocytes. We also thank past and current members of the Yutzey Lab for assistance in harvest of pig cardiac tissues as well as valuable discussions.

Funding

This work was supported by the National Institutes of Health [R01HL135848, R01HL142217 to KEY]; the American Heart Association Predoctoral Fellowship [19PRE34380046 to NV]; and the Cincinnati Children's Hospital Research Foundation.

References

[1]. Benjamin EJ, Muntner P, Alonso A, Bittencourt MS, Callaway CW, Carson AP, Chamberlain AM, Chang AR, Cheng S, Das SR, Delling FN, Djousse L, Elkind MSV, Ferguson JF, Fornage M, Jordan LC, Khan SS, Kissela BM, Knutson KL, Kwan TW, Lackland DT, Lewis TT, Lichtman JH, Longenecker CT, Loop MS, Lutsey PL, Martin SS, Matsushita K, Moran AE, Mussolino ME, O'Flaherty M, Pandey A, Perak AM, Rosamond WD, Roth GA, Sampson UKA, Satou GM, Schroeder EB, Shah SH, Spartano NL, Stokes A, Tirschwell DL, Tsao CW, Turakhia MP, VanWagner LB, Wilkins JT, Wong SS, Virani SS, American E Heart Association Council on, C. Prevention Statistics, S. Stroke Statistics, Heart Disease and Stroke Statistics-2019 Update: A Report From the American Heart Association, Circulation 139(10) (2019) e56–e528. [PubMed: 30700139]

[2]. Lelovas PP, Kostomitsopoulos NG, Xanthos TT, A comparative anatomic and physiologic overview of the porcine heart, J Am Assoc Lab Anim Sci 53(5) (2014) 432–8. [PubMed: 25255064]

[3]. Kang MJ, Kim JS, Chae SW, Koh KN, Koh GY, Cyclins and cyclin dependent kinases during cardiac development, Mol Cells 7(3) (1997) 360–6. [PubMed: 9264023]

[4]. Hesse M, Welz A, Fleischmann BK, Heart regeneration and the cardiomyocyte cell cycle, Pflugers Arch 470(2) (2018) 241–248. [PubMed: 28849267]

[5]. Li F, Wang X, Capasso JM, Gerdes AM, Rapid transition of cardiac myocytes from hyperplasia to hypertrophy during postnatal development, J Mol Cell Cardiol 28(8) (1996) 1737–46. [PubMed: 8877783]

[6]. Soonpaa MH, Kim KK, Pajak L, Franklin M, Field LJ, Cardiomyocyte DNA synthesis and binucleation during murine development, Am J Physiol 271(5 Pt 2) (1996) H2183–9. [PubMed: 8945939]

[7]. Yin Z, Ren J, Guo W, Sarcomeric protein isoform transitions in cardiac muscle: a journey to heart failure, Biochim Biophys Acta 1852(1) (2015) 47–52. [PubMed: 25446994]

[8]. Puente BN, Kimura W, Muralidhar SA, Moon J, Amatruda JF, Phelps KL, Grinsfelder D, Rothermel BA, Chen R, Garcia JA, Santos CX, Thet S, Mori E, Kinter MT, Rindler PM, Zacchigna S, Mukherjee S, Chen DJ, Mahmoud AI, Giacca M, Rabinovitch PS, Aroumougame A, Shah AM, Szweda LI, Sadek HA, The oxygen-rich postnatal environment induces cardiomyocyte cell-cycle arrest through DNA damage response, Cell 157(3) (2014) 565–79. [PubMed: 24766806]

[9]. Yahalom-Ronen Y, Rajchman D, Sarig R, Geiger B, Tzahor E, Reduced matrix rigidity promotes neonatal cardiomyocyte dedifferentiation, proliferation and clonal expansion, Elife 4 (2015).

[10]. He L, Huang X, Kanisicak O, Li Y, Wang Y, Li Y, Pu W, Liu Q, Zhang H, Tian X, Zhao H, Liu X, Zhang S, Nie Y, Hu S, Miao X, Wang QD, Wang F, Chen T, Xu Q, Lui KO, Molkentin JD, Zhou B, Preexisting endothelial cells mediate cardiac neovascularization after injury, J Clin Invest 127(8) (2017) 2968–2981. [PubMed: 28650345]

[11]. Horackova M, Slavikova J, Byczko Z, Postnatal development of the rat intrinsic cardiac nervous system: a confocal laser scanning microscopy study in whole-mount atria, Tissue Cell 32(5) (2000) 377–88. [PubMed: 11201277]

[12]. Aurora AB, Porrello ER, Tan W, Mahmoud AI, Hill JA, Bassel-Duby R, Sadek HA, Olson EN, Macrophages are required for neonatal heart regeneration, J Clin Invest 124(3) (2014) 1382–92. [PubMed: 24569380]

[13]. Porrello ER, Olson EN, A neonatal blueprint for cardiac regeneration, Stem Cell Res 13(3 Pt B) (2014) 556–70. [PubMed: 25108892]

[14]. Ye L, D'Agostino G, Loo SJ, Wang CX, Su LP, Tan SH, Tee GZ, Pua CJ, Pena EM, Cheng RB, Chen WC, Abdurrachim D, Lalic J, Tan RS, Lee TH, Zhang J, Cook SA, Early Regenerative Capacity in the Porcine Heart, Circulation 138(24) (2018) 2798–2808. [PubMed: 30030417]

[15]. Zhu W, Zhang E, Zhao M, Chong Z, Fan C, Tang Y, Hunter JD, Borovjagin AV, Walcott GP, Chen JY, Qin G, Zhang J, Regenerative Potential of Neonatal Porcine Hearts, Circulation 138(24) (2018) 2809–2816. [PubMed: 30030418]

[16]. Mollova M, Bersell K, Walsh S, Savla J, Das LT, Park SY, Silberstein LE, Dos Remedios CG, Graham D, Colan S, Kuhn B, Cardiomyocyte proliferation contributes to heart growth in young humans, Proc Natl Acad Sci U S A 110(4) (2013) 1446–51. [PubMed: 23302686]

[17]. Patterson M, Barske L, Van Handel B, Rau CD, Gan P, Sharma A, Parikh S, Denholtz M, Huang Y, Yamaguchi Y, Shen H, Allayee H, Crump JG, Force TI, Lien CL, Makita T, Lusis AJ, Kumar SR, Sucov HM, Frequency of mononuclear diploid cardiomyocytes underlies natural variation in heart regeneration, Nat Genet 49(9) (2017) 1346–1353. [PubMed: 28783163]

[18]. Livak KJ, Schmittgen TD, Analysis of relative gene expression data using real-time quantitative PCR and the 2(-Delta Delta C(T)) Method, Methods 25(4) (2001) 402–8. [PubMed: 11846609]

[19]. Kim D, Langmead B, Salzberg SL, HISAT: a fast spliced aligner with low memory requirements, Nat Methods 12(4) (2015) 357–60. [PubMed: 25751142]

[20]. Risso D, Ngai J, Speed TP, Dudoit S, Normalization of RNA-seq data using factor analysis of control genes or samples, Nat Biotechnol 32(9) (2014) 896–902. [PubMed: 25150836]

[21]. Chen J, Bardes EE, Aronow BJ, Jegga AG, ToppGene Suite for gene list enrichment analysis and candidate gene prioritization, Nucleic Acids Res 37(Web Server issue) (2009) W305–11. [PubMed: 19465376]

[22]. Foglia MJ, Poss KD, Building and re-building the heart by cardiomyocyte proliferation, Development 143(5) (2016) 729–40. [PubMed: 26932668]

[23]. Gourdie RG, Green CR, Severs NJ, Thompson RP, Immunolabelling patterns of gap junction connexins in the developing and mature rat heart, Anat Embryol (Berl) 185(4) (1992) 363–78. [PubMed: 1319120]

[24]. Saggin L, Gorza L, Ausoni S, Schiaffino S, Troponin I switching in the developing heart, J Biol Chem 264(27) (1989) 16299–302. [PubMed: 2777792]

[25]. Grabner W, Pfitzer P, Number of nuclei in isolated myocardial cells of pigs, Virchows Arch B Cell Pathol 15(4) (1974) 279–94. [PubMed: 4135954]

[26]. Hirose K, Payumo AY, Cutie S, Hoang A, Zhang H, Guyot R, Lunn D, Bigley RB, Yu H, Wang J, Smith M, Gillett E, Muroy SE, Schmid T, Wilson E, Field KA, Reeder DM, Maden M, Yartsev MM, Wolfgang MJ, Grutzner F, Scanlan TS, Szweda LI, Buffenstein R, Hu G, Flamant F, Olgin JE, Huang GN, Evidence for hormonal control of heart regenerative capacity during endothermy acquisition, Science 364(6436) (2019) 184–188. [PubMed: 30846611]

[27]. Bergmann O, Bhardwaj RD, Bernard S, Zdunek S, Barnabe-Heider F, Walsh S, Zupicich J, Alkass K, Buchholz BA, Druid H, Jovinge S, Frisen J, Evidence for cardiomyocyte renewal in humans, Science 324(5923) (2009) 98–102. [PubMed: 19342590]

[28]. Adler CP, Friedburg H, Herget GW, Neuburger M, Schwalb H, Variability of cardiomyocyte DNA content, ploidy level and nuclear number in mammalian hearts, Virchows Arch 429(2–3) (1996) 159–64. [PubMed: 8917717]

[29]. Han L, Choudhury S, Mich-Basso JD, Ammanamanchi N, Ganapathy B, Suresh S, Khaladkar M, Singh J, Maehr R, Zuppo DA, Kim J, Eberwine JH, Wyman SK, Wu YL, Kuhn B, Lamin B2 Levels Regulate Polyploidization of Cardiomyocyte Nuclei and Myocardial Regeneration, Dev Cell (2020).

[30]. Liu H, Zhang CH, Ammanamanchi N, Suresh S, Lewarchik C, Rao K, Uys GM, Han L, Abrial M, Yimlamai D, Ganapathy B, Guillermier C, Chen N, Khaladkar M, Spaethling J, Eberwine JH, Kim J, Walsh S, Choudhury S, Little K, Francis K, Sharma M, Viegas M, Bais A, Kostka D, Ding

J, Bar-Joseph Z, Wu Y, Yechoor V, Moulik M, Johnson J, Weinberg J, Reyes-Mugica M, Steinhauser ML, Kuhn B, Control of cytokinesis by beta-adrenergic receptors indicates an approach for regulating cardiomyocyte endowment, Sci Transl Med 11(513) (2019).

[31]. Hashmi S, Ahmad HR, Molecular switch model for cardiomyocyte proliferation, Cell Regen (Lond) 8(1) (2019) 12–20.

[32]. Sengupta A, Kalinichenko VV, Yutzey KE, FoxO1 and FoxM1 transcription factors have antagonistic functions in neonatal cardiomyocyte cell-cycle withdrawal and IGF1 gene regulation, Circ Res 112(2) (2013) 267–77. [PubMed: 23152492]

[33]. Ascuitto RJ, Ross-Ascuitto NT, Substrate metabolism in the developing heart, Semin Perinatol 20(6) (1996) 542–63. [PubMed: 9090780]

[34]. Lopaschuk GD, Jaswal JS, Energy metabolic phenotype of the cardiomyocyte during development, differentiation, and postnatal maturation, J Cardiovasc Pharmacol 56(2) (2010) 130–40. [PubMed: 20505524]

[35]. Shao D, Tian R, Glucose Transporters in Cardiac Metabolism and Hypertrophy, Compr Physiol 6(1) (2015) 331–51. [PubMed: 26756635]

[36]. Mahmoud AI, O'Meara CC, Gemberling M, Zhao L, Bryant DM, Zheng R, Gannon JB, Cai L, Choi WY, Egnaczyk GF, Burns CE, Burns CG, MacRae CA, Poss KD, Lee RT, Nerves Regulate Cardiomyocyte Proliferation and Heart Regeneration, Dev Cell 34(4) (2015) 387–99. [PubMed: 26256209]

[37]. Porrello ER, Mahmoud AI, Simpson E, Hill JA, Richardson JA, Olson EN, Sadek HA, Transient regenerative potential of the neonatal mouse heart, Science 331(6020) (2011) 1078–80. [PubMed: 21350179]

[38]. Mohamed TMA, Ang YS, Radzinsky E, Zhou P, Huang Y, Elfenbein A, Foley A, Magnitsky S, Srivastava D, Regulation of Cell Cycle to Stimulate Adult Cardiomyocyte Proliferation and Cardiac Regeneration, Cell 173(1) (2018) 104–116 e12. [PubMed: 29502971]

[39]. Jiang YH, Zhu Y, Chen S, Wang HL, Zhou Y, Tang FQ, Jian Z, Xiao YB, Re-enforcing hypoxia-induced polyploid cardiomyocytes enter cytokinesis through activation of beta-catenin, Sci Rep 9(1) (2019) 17865. [PubMed: 31780774]

[40]. Gan P, Patterson M, Sucov HM, Cardiomyocyte Polyploidy and Implications for Heart Regeneration, Annu Rev Physiol 82 (2020) 45–61. [PubMed: 31585517]

[41]. Matrone G, Tucker CS, Denvir MA, Cardiomyocyte proliferation in zebrafish and mammals: lessons for human disease, Cell Mol Life Sci 74(8) (2017) 1367–1378. [PubMed: 27812722]

[42]. Gonzalez-Rosa JM, Sharpe M, Field D, Soonpaa MH, Field LJ, Burns CE, Burns CG, Myocardial Polyploidization Creates a Barrier to Heart Regeneration in Zebrafish, Dev Cell 44(4) (2018) 433–446 e7. [PubMed: 29486195]

[43]. Agnew EJ, Velayutham N, Matos Ortiz G, Alfieri CM, Hortells L, Moore V, Riggs KW, Baker RS, Gibson AM, Ponny SR, Alsaied T, Zafar F, Yutzey KE, Scar Formation with Decreased Cardiac Function Following Ischemia/Reperfusion Injury in 1 Month Old Swine, J Cardiovasc Dev Dis 7(1) (2019).

[44]. Nakada Y, Canseco DC, Thet S, Abdisalaam S, Asaithamby A, Santos CX, Shah AM, Zhang H, Faber JE, Kinter MT, Szweda LI, Xing C, Hu Z, Deberardinis RJ, Schiattarella G, Hill JA, Oz O, Lu Z, Zhang CC, Kimura W, Sadek HA, Hypoxia induces heart regeneration in adult mice, Nature 541(7636) (2017) 222–227. [PubMed: 27798600]

[45]. Burrell JH, Boyn AM, Kumarasamy V, Hsieh A, Head SI, Lumbers ER, Growth and maturation of cardiac myocytes in fetal sheep in the second half of gestation, Anat Rec A Discov Mol Cell Evol Biol 274(2) (2003) 952–61. [PubMed: 12973719]

[46]. Velayutham N, Agnew EJ, Yutzey KE, Postnatal Cardiac Development and Regenerative Potential in Large Mammals, Pediatr Cardiol (2019).

[47]. Li JW, Hu J, Wei M, Guo YY, Yan PS, The Effects of Maternal Obesity on Porcine Placental Efficiency and Proteome, Animals (Basel) 9(8) (2019).

[48]. Bassat E, Mutlak YE, Genzelinakh A, Shadrin IY, Baruch Umansky K, Yifa O, Kain D, Rajchman D, Leach J, Riabov Bassat D, Udi Y, Sarig R, Sagi I, Martin JF, Bursac N, Cohen S, Tzahor E, The extracellular matrix protein agrin promotes heart regeneration in mice, Nature 547(7662) (2017) 179–184. [PubMed: 28581497]

[49]. Wang J, Karra R, Dickson AL, Poss KD, Fibronectin is deposited by injury-activated epicardial cells and is necessary for zebrafish heart regeneration, Dev Biol 382(2) (2013) 427–35. [PubMed: 23988577]

[50]. Li F, McNelis MR, Lustig K, Gerdes AM, Hyperplasia and hypertrophy of chicken cardiac myocytes during posthatching development, Am J Physiol 273(2 Pt 2) (1997) R518–26. [PubMed: 9277534]

Highlights

- Pig cardiomyocyte (CM) maturation and mitotic arrest occur over 2–6 months.
- Nearly 50% mononucleated-diploid CMs persist at 2 weeks after birth in swine.
- Adolescent pig CMs exhibit progressive multinucleation and longitudinal growth.
- Pig CM terminal maturation does not coincide with reported P3 regenerative loss.
- RNAseq suggests critical role for non-CM factors in postnatal pig heart maturation.

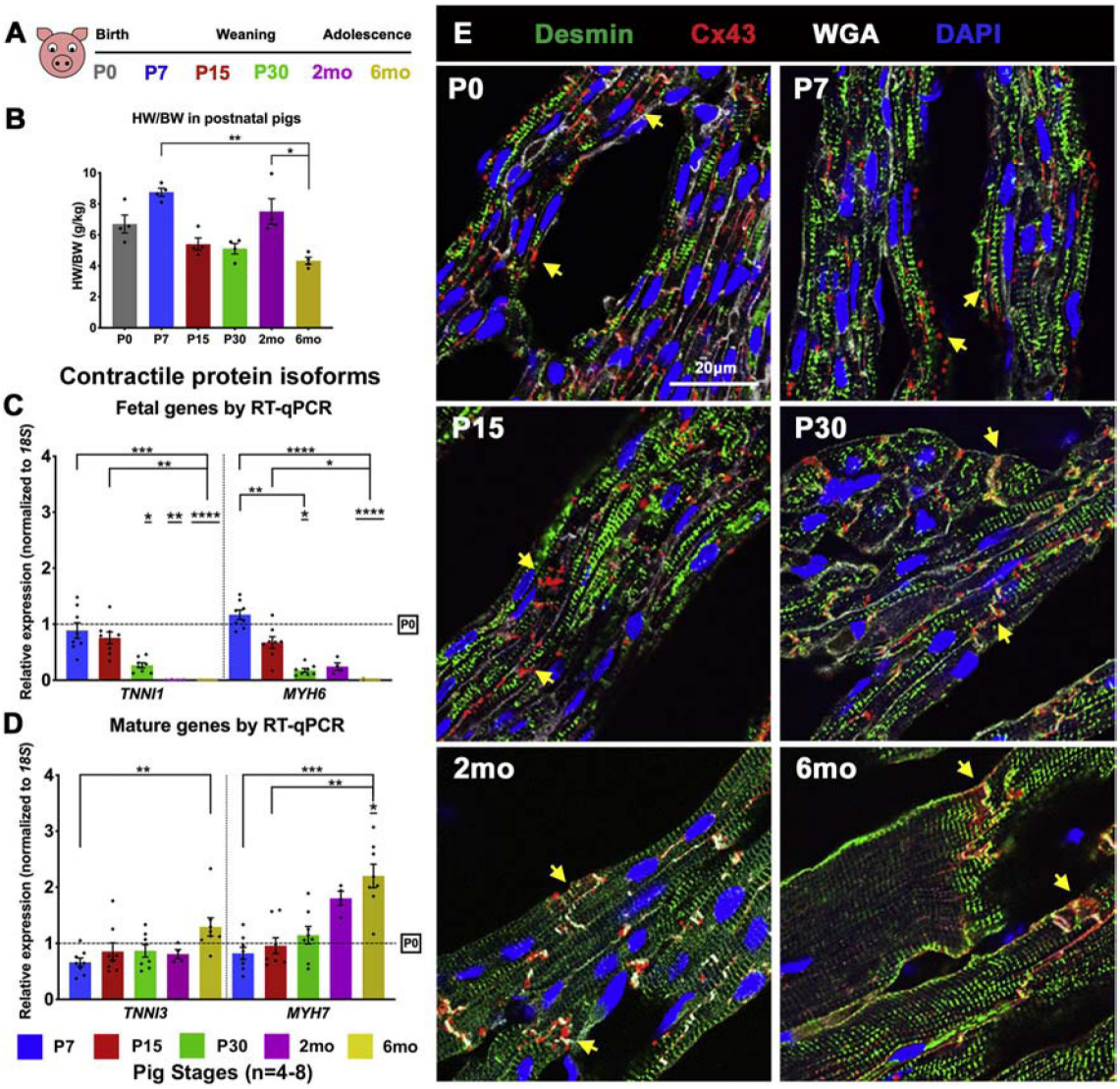

Figure 1. Cardiac myocyte sarcomeric and gap junctional maturation occur beyond P30 in pigs.

(A) Schematic of pig heart stages utilized for this study. **(B)** Heart weight/body weight (HW/BW in g/kg) ratios were calculated for pigs at P0–6mo. **(C, D)** Expression of cardiac contractile protein fetal and mature isoforms at P7–6mo in pig left ventricles, with fold change relative to P0. **(E)** Representative images of Connexin-43 (Cx43) staining of gap junction proteins. Yellow arrows show change in Cx43 expression from lateral punctate staining at P0-P15 to co-localization at CM termini at P30–6mo. Data are mean ± SEM, with *p<0.05, **p<0.01, ***p<0.001, ****p<0.0001 determined by Dunn's Kruskal-Wallis Multiple Comparisons Tests, in n=4–8 pigs per stage. Asterisk(s) with underline indicate significance compared to P0.

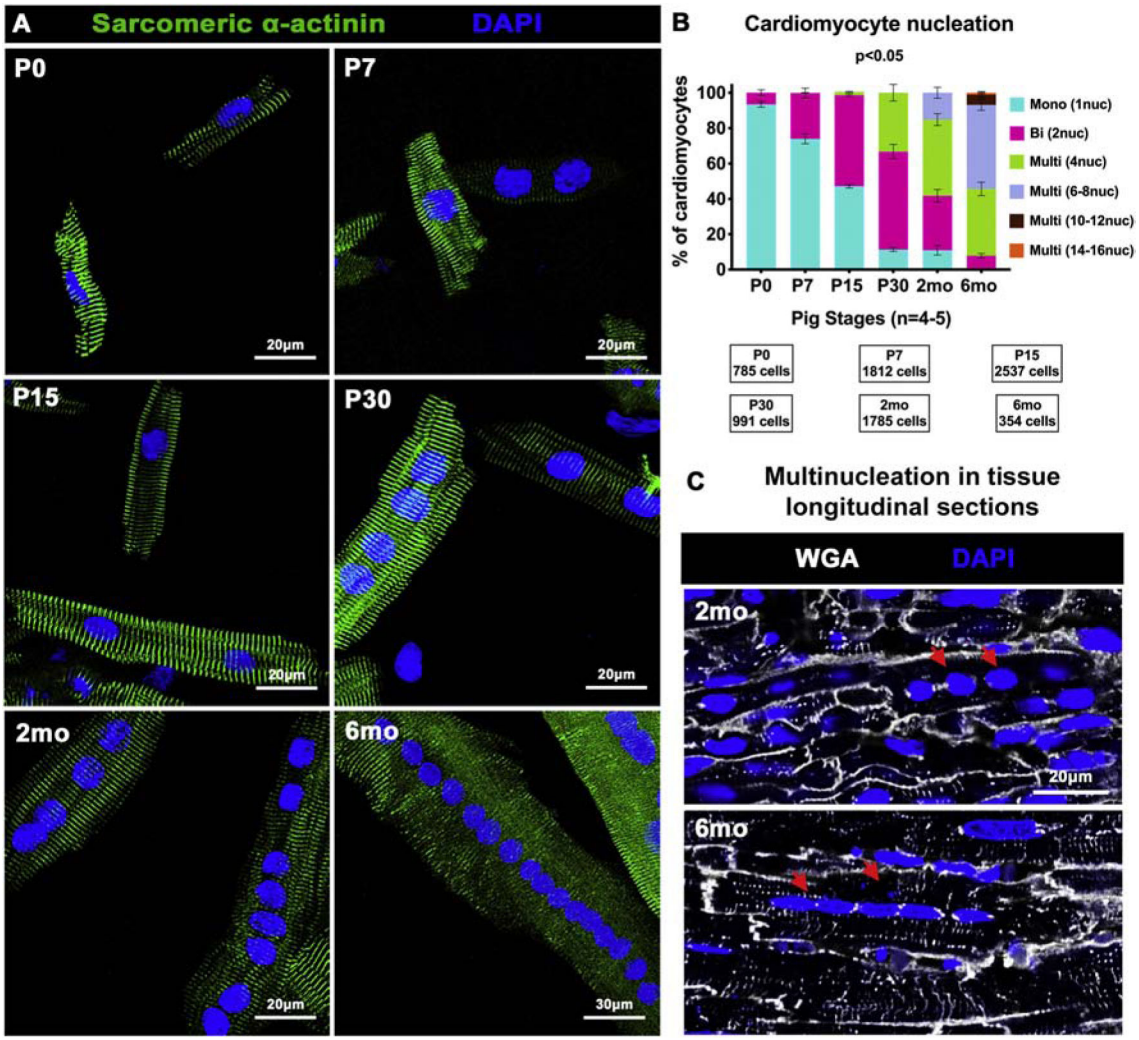

Figure 2. Postnatal pig CMs exhibit progressive multinucleation from P15–6mo, with significant mononucleation until P15.

(A) Representative images of pig dissociated CMs from P0 to 6mo showing nucleation by DAPI staining (blue), with CMs identified by sarcomeric α-actinin (green). **(B)** Percentage of total CMs exhibiting mono-, bi-, and multi-nucleation per stage calculated by manual nucleation counts. **(C)** Representative images of multinucleated CMs (red arrows), via WGA staining in longitudinal sections of pig left ventricular tissue. Data are mean ± SEM, with $p<0.05$ determined by Dunn's Kruskal-Wallis Multiple Comparisons Test in n=4–5 pigs per stage.

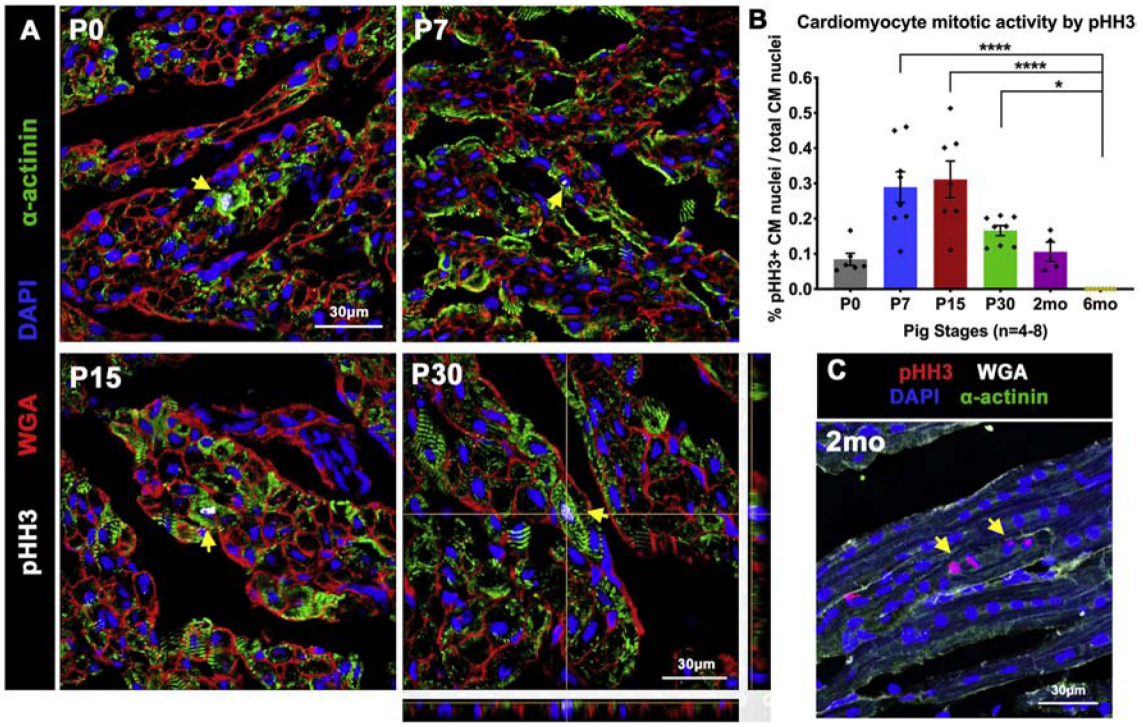

Figure 3. CM mitotic activity is detected up to 2mo in postnatal pig hearts.

(A) Representative images of Phosphohistone-H3 (pHH3) staining for mitotic activity (yellow arrows) in pig heart tissue sections, with CMs identified by sarcomeric α-actinin. P30 image showing representative Z-stack planes indicates the analysis method used to accurately identify CMs at all stages. **(B)** Representative longitudinal tissue section showing multinucleated CM with simultaneous pHH3 activation in adjacent nuclei (yellow arrows). **(C)** Ratio of pHH3-positive CM nuclei to total CM nuclei was calculated in cardiac cross-sections. Data are mean ± SEM, with *p<0.05, **p<0.01, ***p<0.001, ****p<0.0001 determined by Dunn's Kruskal-Wallis Multiple Comparisons Tests in n=4–8 pigs per stage.

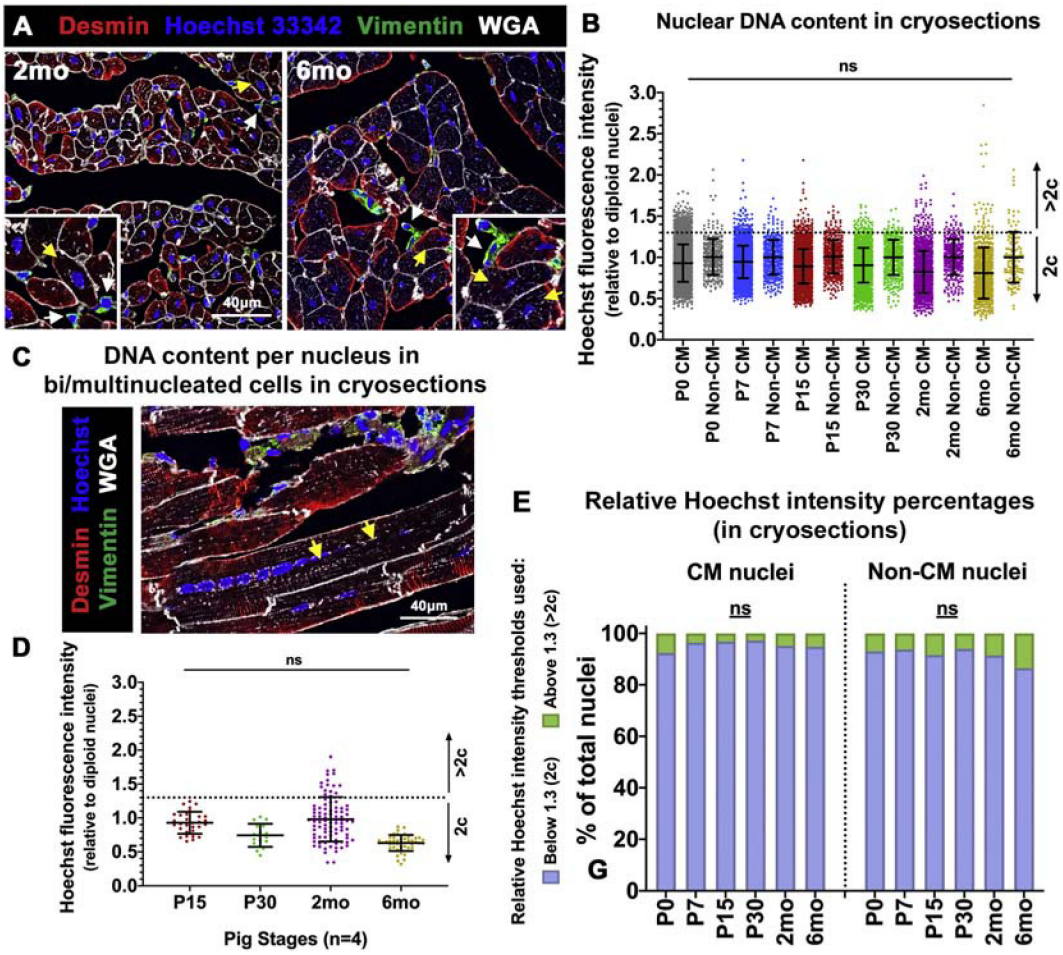

Figure 4. Pig CM nuclei remain predominantly diploid after birth.

(A) Representative images of ventricular tissue cryosections stained with Hoechst 33342 for CM nuclear intensity assessment (yellow arrows), with Vimentin-positive non-CM cell nuclei (white arrows) utilized as diploid (2c) control. **(B)** Hoechst fluorescence intensity per CM nucleus, relative to Vimentin-positive non-CM nuclear Hoechst intensities, was calculated per image. Thresholds for 2c and >2c were determined based on standard deviation of non-CM (2c) nuclei (>100 CMs analyzed per stage). **(C)** Representative image of a multinucleated CM (yellow arrows) in longitudinal tissue section stained with Desmin, Hoechst, and WGA, for nuclear intensity measurements. **(D)** Hoechst fluorescence intensity per nucleus in multinucleated CMs was measured at P15–6mo in cryosections. **(E)** Percentages of CM and non-CM nuclei with relative Hoechst intensities at 2c or >2c, as determined in tissue longitudinal cryosections. Data are mean ± SEM, with ns=not significant determined compared to P0 by Brown-Forsythe and Welch ANOVA tests, in n=4 pigs per stage.

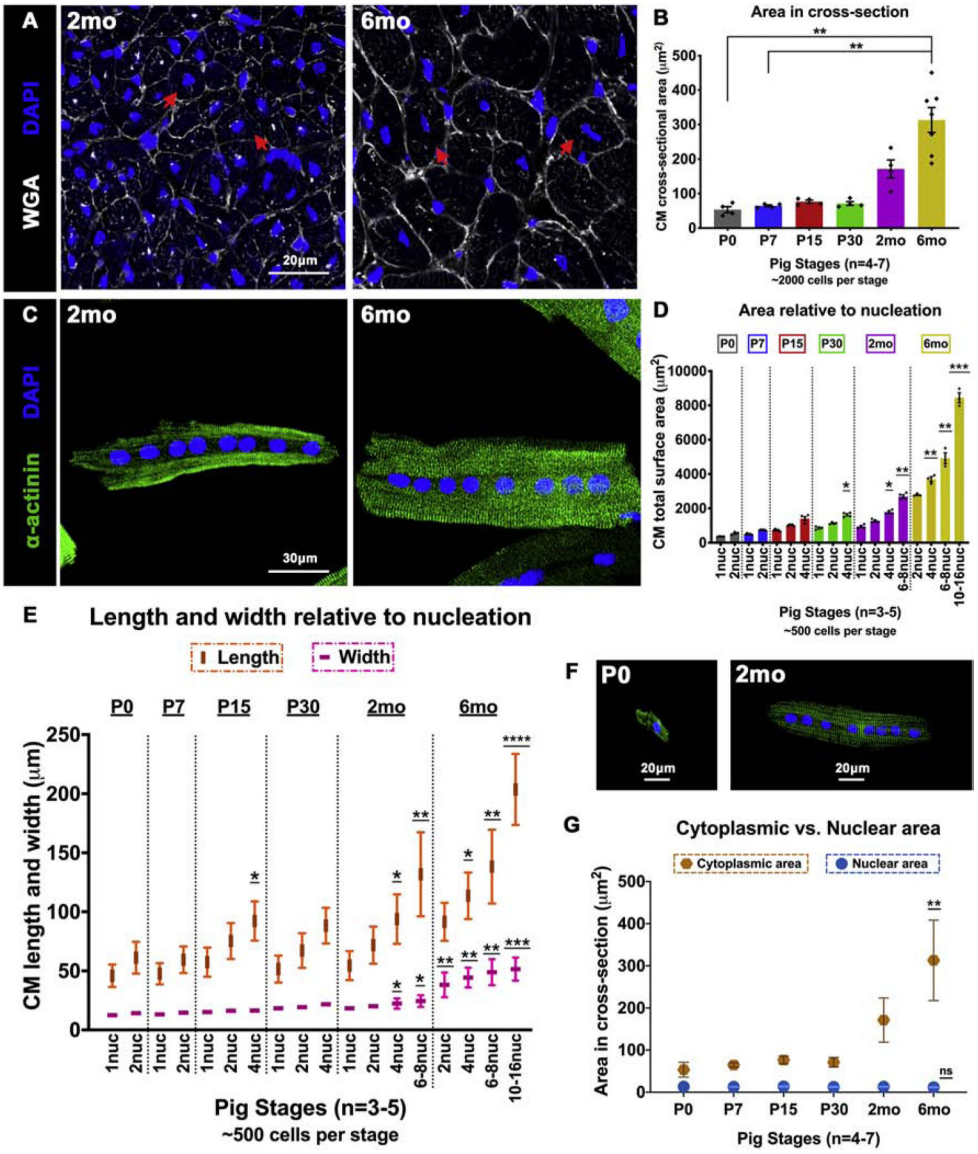

Figure 5. CM length increases relative to nucleation beyond while CM width does not increase until 2mo-6mo in postnatal pigs.

(A) Representative images of pig heart cross-sections stained with WGA and DAPI at 2mo and 6mo. Red arrows indicate increase in CM cross-sectional cell size. **(B)** CM cross-sectional area (μm^2) in paraffin sections was quantified by manual cell tracing based on WGA staining. **(C)** Representative images of dissociated pig CMs showing increased size between octanucleated cells at 2mo and 6mo. **(D)** Total surface area (μm^2) was measured by manual cell tracing of dissociated CMs based on α-actinin staining. **(E)** Length and width were assessed in dissociated pig CMs by manual measurements. **(F)** Representative images of change in CM length relative to nucleation at P0 and 2mo. **(G)** Nuclear area based on DAPI staining was measured and compared against cytoplasmic area measured by cell tracing in WGA-stained paraffin cross-sections. Data are mean ± SEM in B and D, and mean ± SD in E, with *p<0.05, **p<0.01, ***p<0.001, ****p<0.0001 determined by Dunn's Kruskal-Wallis Multiple Comparisons Tests. Asterisk(s) with underline indicate

significance compared to mononucleated P0 CM (P0–1nuc) in D and E. In G, data are mean ± SD, with **p<0.01 and ns=not significant determined compared to P0 by Brown-Forsythe and Welch ANOVA tests with Games-Howell corrections for Multiple Comparisons, in n=3–7 pigs per stage.

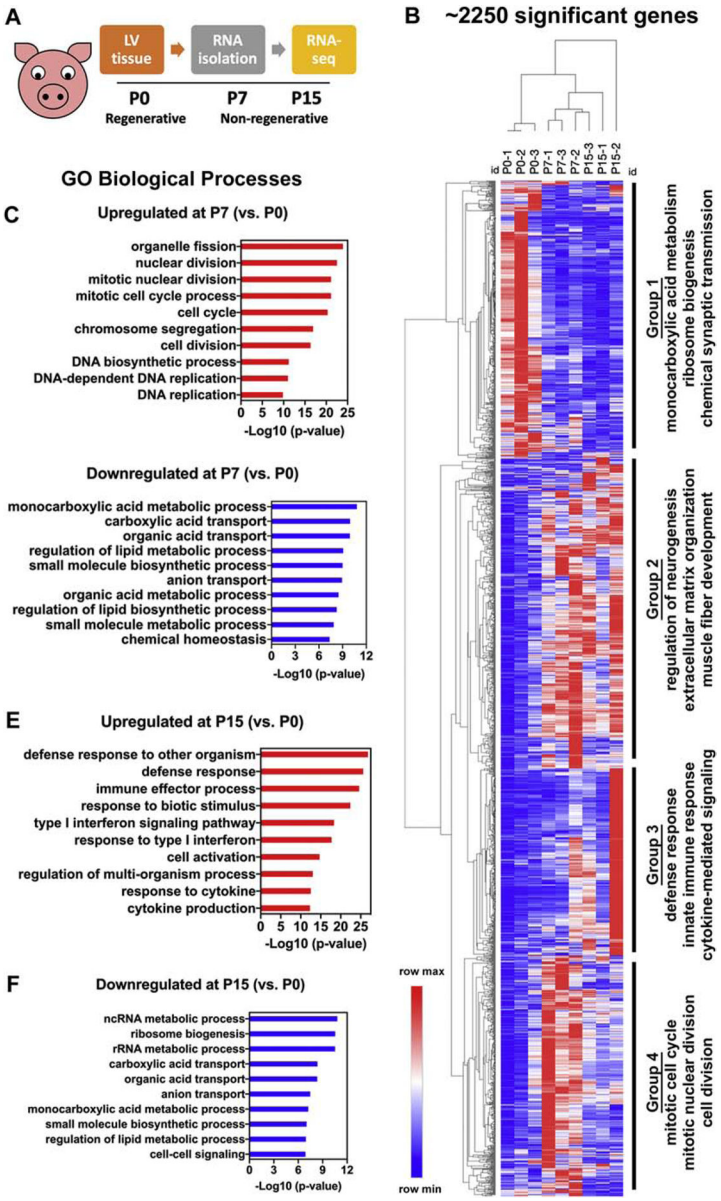

Figure 6. RNAseq indicates upregulation of cell cycling at P7 and immune signaling at P15, alongside downregulation of carboxylic acid metabolic processes, in postnatal swine.

(A) Schematic of RNAseq experimental design. **(B)** Heatmap showing 2253 significantly differentially expressed genes between P0, P7, and P15, categorized into four groups based on GO-biological process (BP) terms. **(C, D)** Top GO-BP terms for significantly upregulated and downregulated genes at P7 compared to P0 (P7 vs. P0). **(E, F)** Top GO-BP terms for significantly upregulated and downregulated genes at P15 compared to P0 (P15 vs. P0). Significant differentially expressed genes were obtained using a fold change cutoff of 2 and adjusted p-value≤0.05, in n=3 pigs per stage.

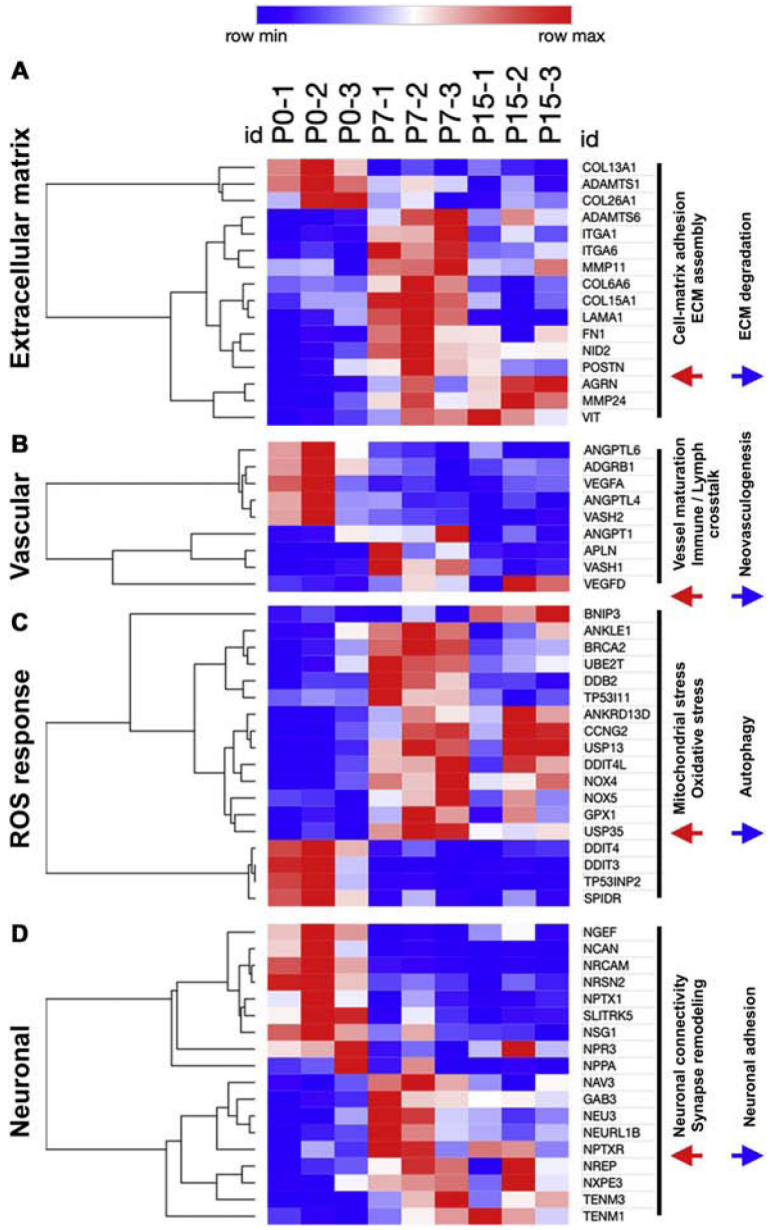

Figure 7. Upregulation of extracellular matrix maturation, ROS response, and sympathetic neuronal regulation in pigs after birth.

Heatmaps showing selected significantly differentially expressed genes between P0, P7, and P15, categorized into four groups based on top GO-BP terms as **(A)** Extracellular matrix (ECM) genes, **(B)** Vascular genes, **(C)** Reactive oxygen species (ROS) responsive genes, and **(D)** Neuronal signaling genes. Significant differentially expressed genes were obtained using a fold change cutoff of 2 and adjusted p-value≤0.05, in n=3 pigs per stage.

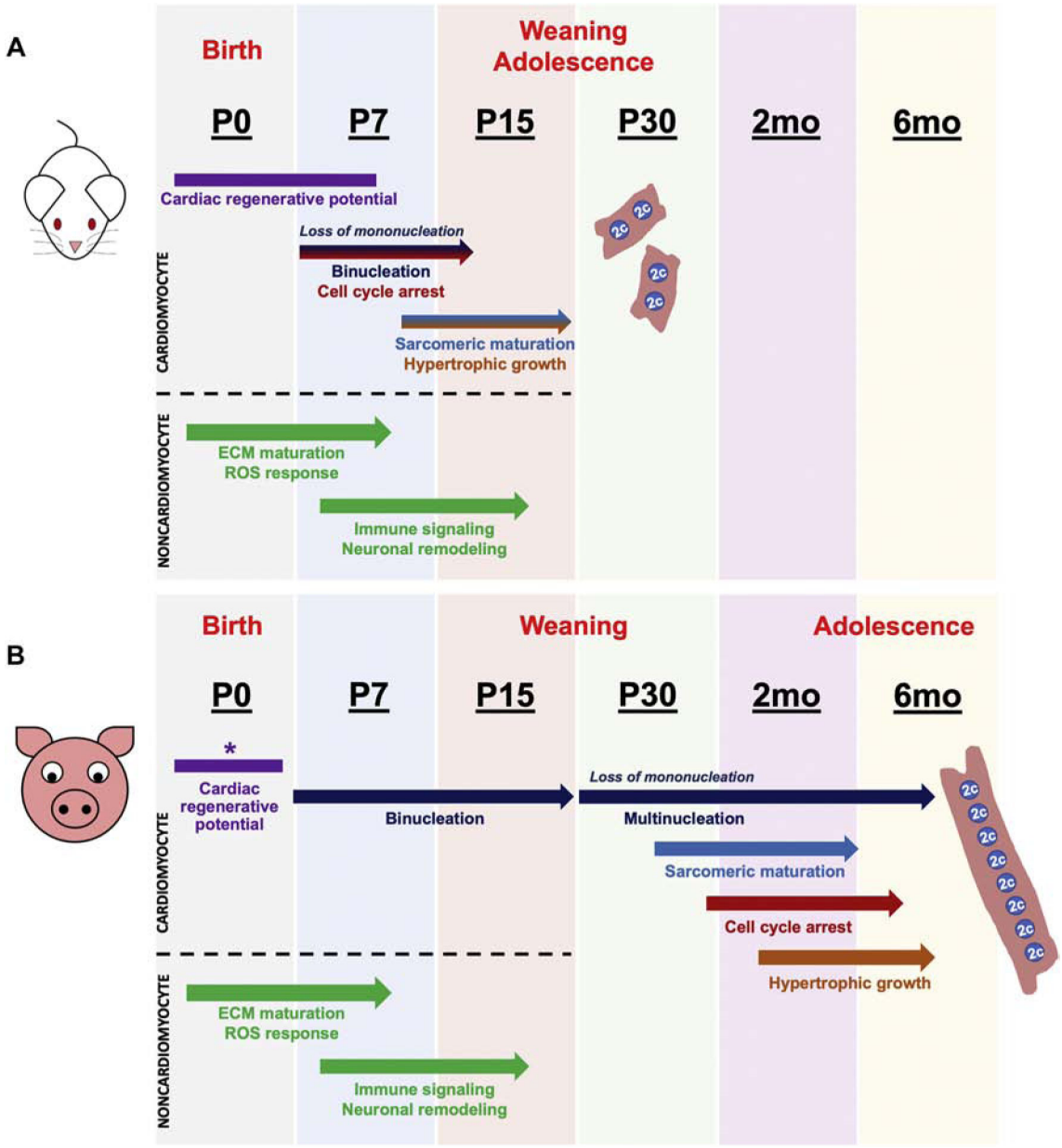

Figure 8. Cardiomyocyte terminal maturation in pigs is delayed compared to mice, despite similar neonatal periods of heart regenerative potential.

(A) Schematic summary of published postnatal developmental events in murine hearts that coincide with loss of cardiac regenerative capacity at P7. **(B)** Scheme summarizing our results, where postnatal pig hearts display discordant timing of cardiomyocyte maturational milestones compared to loss of regenerative capacity at P3. Transcriptomic changes in extracellular matrix, immune signaling, sympathetic neuron remodeling, and ROS response are conserved during transition from a regenerative to a non-regenerative postnatal heart in both mice and pigs. *Pig cardiac regenerative window is as described in previous reports [14, 15].